This article has been accepted for publication in a future issue of this journal, but has not been fully edited. Content may change prior to final publication. Citation information: DOI 10.1109/TIE.2018.2821109, IEEE Transactions on Industrial Electronics

Effects of Design Parameters on Performance of Brushless Electrically Excited Synchronous Reluctance Generator

Fengge Zhang, *Member*, *IEEE*, Hao Wang, Guanglong Jia, Dandan Ma, and Milutin G. Jovanovic, *Senior member*, *IEEE*

***Abstract*—Permanent magnet synchronous generators, doubly fed induction generators, and traditional electrically excited synchronous generators are widely used for wind power applications, especially large offshore installations. In order to eliminate brushes and slip rings for improved reliability and maintenance-free operation, as well as to avoid costly permanent magnets, a novel brushless electrically excited synchronous reluctance generator having many outstanding advantages has been proposed in this paper. The fundamental operating principles, finite element analysis design studies and performance optimization aspects have been thoroughly investigated by simulations and experimentally under different loading conditions. The effects of different pole combinations and rotor dimensions on the magnetic coupling capacity of this machine have been specifically addressed and fully verified by off-line testing of the 6/2 pole and 8/4 pole prototypes with magnetic barrier reluctance rotor and a new hybrid cage rotor offering superior performance.**

***Index Terms*—Stator electrically excited, brushless synchronous reluctance generator, pole combinations, rotor dimensions, coupling capacity, performance analysis.**

NOMENCLATURE

p	Pole-pairs of the armature winding (AW)
q	Pole-pairs of the excitation winding (EW)
n_r	Rotor speed [rev/min]
f	Frequency of the AW [Hz]
p_r	Rotor pole number of the BEESRG
IPM	Intelligent power module
P_{sAW}, P_{sEW}	Slip power of the AW, EW
P_{emAW}, P_{emEW}	Electromagnetic power of the AW, EW
s_{AW}, s_{EW}	Percentage slip value of the AW, EW
n_{AW}, n_{EW}	Magnetic field rotation speed of the AW, EW [rev/min]
P_{mecAW}, P_{mecEW}	Mechanical power of the AW, EW
λ	Ratio of magnetic and non-magnetic layer
β	Useful harmonic content
VRR	Voltage regulation rate
T_{em}	Torque of the BEESRG
L	Mutual inductance between the AW and EW
i_{AW}, i_{EW}	Current magnitude of the AW, EW
γ	Angle between the induced phase voltage and current

Manuscript received October 30, 2017; revised February 05, 2018; accepted March 04, 2018. This work was supported by Key Project of National Natural Science Foundation of China under Grant 51537007.

Fengge Zhang, Hao Wang, and Dandan Ma are with the school of Electrical Engineering, Shenyang University of Technology, Shenyang, 110870, China (e-mail: zhangfg@sut.edu.cn, wanghao8224@163.com, 2514242781@qq.com).

Guanglong Jia is with CRRC Zhuzhou Institute Co.Ltd, Zhuzhou, 412001, China (Email: jiaguanglong_87@163.com)

Milutin G. Jovanovic is with the Department of Physics and Electrical Engineering, Northumbria University, Newcastle upon Tyne NE1 8ST, U. K. (Email: milutin.jovanovic@northumbria.ac.uk).

I. INTRODUCTION

SIGNIFICANT market volatility and other disadvantages of permanent magnets have stimulated existing research on more economical alternative technologies for commercial large-scale wind energy conversion systems (WECS), the conventional doubly-fed induction generator (DFIG) and the electrically excited synchronous generator (EESG). While the DFIG has apparent cost benefits of using a partially-rated converter, it cannot compete favorably with the prevailing permanent magnet generators (PMGs) or EESGs in terms of efficiency and especially the grid-code compliance under fault conditions. The EESGs, on the other hand, largely retain most of the PMGs merits such as high torque density and efficiency, and superior grid-integration properties e.g. low voltage ride through (LVRT) capabilities. However, an obvious drawback of both EESG and DFIG relative to the PMG are the reliability issues and higher operation & maintenance requirements with the presence of brushes and slip rings.

In order to overcome the above EESG limitations, brushless excitation techniques have been receiving more attention, and many interesting original design solutions have been recently considered for either motoring or generating operation [1-3]. A variable-speed constant-frequency system based on a wound rotor synchronous generator with a brushless exciter has been investigated in [4]. A novel structure of the brushless electrically excited motor with the improved power density and controllability is suggested in [5]. The brushless synchronous machine with a 3-phase open winding configuration and dual

(i.e., AC and DC) excitation is put forward in [6]. In [7], a novel stator excited synchronous machine without rare-earth magnets, slip rings or brushes is presented. In [8], a new type of the dual-stator brushless doubly-fed induction generator for wind turbines is proposed. A brushless synchronous machine with additional harmonic field stator and rotor windings, namely the double harmonic windings excitation synchronous machine, has been introduced in [9]. In [10], a magnetic-field-modulated brushless double-rotor machine having the modulating ring and permanent magnet rotors is proposed. Low-power brushless permanent magnet machines for automotive applications have been considered in [11,12]. A brushless claw-pole double rotor machine for power split hybrid electric vehicles with a higher slot fill factor, lower copper loss, and fault tolerant capacity is suggested in [13]. A brushless excitation approach using ceramic insulated sleeve bearings with oil lubrication to form capacitive coupling of the slip rings is presented in [14]. A separately excited synchronous motor with a rotary transformer for hybrid vehicles is introduced in [15]. A high power density wound field synchronous machine for electric vehicle traction drives is presented in [16].

In this paper, a novel magnet-free version of the EESG, termed as the brushless electrically excited synchronous reluctance generator (BEESRG), is proposed based on the traditional EESG and emerging brushless doubly fed generator (BDFG) topologies. As a hybrid design, the BEESRG has inherited most of the EESG and/or BDFG advantages whilst bringing additional benefits. Compared with the EESG, the BEESRG can offer much enhanced reliability and significant reductions of the maintenance costs and drive train downtime by avoiding regular brush replacements and servicing routines. The absence of expensive rare-earth permanent magnets (e.g. NdFeB) and associated risks of irreversible demagnetization with increasing operating temperatures renders it more cost-effective and reliable than the PMG. Similarly to the EESG and PMG, a fully-rated power electronics converter interface with the supply grid allows better LVRT performance and controllability than either the BDFG or DFIG. Besides, the BEESRG is naturally a medium to low speed machine implying that the vulnerable high-speed stage of geared DFIGs becomes redundant as with the BDFG. Such attractive features make it a good candidate for grid-connected wind turbines.

The main structural difference between the BEESRG and classical EESG is that the excitation winding is placed on the stator and not on the rotor, so that the slip rings and brushes are no longer necessary and can be eliminated in much the same manner as with the BDFG. There are therefore two stator windings of different pole numbers, i.e., the 2p-pole armature winding (AW) and 2q-pole excitation winding (EW) which magnetically couple indirectly through a specially designed rotor by analogy to the BDFG [17]. However, unlike the latter having two standard 3-phase symmetric windings, the AW and EW of the BEESRG are 3-phase and single-phase, respectively.

The paper is organized as follows. In Section II, the basic steady-state theory, operating principles and the fundamental power flow relationships for the BEESRG are introduced. The effects of the main design parameters and winding functions such as pole number combinations, excitation modes, and different reluctance and cage assisted rotor structures on the BEESRG magnetic coupling are examined by comparative simulation studies in Section III. In Section IV, the simulation models for the 6/2 pole and 8/4 pole BEESRGs with the magnetic barrier and hybrid cage rotor designs have been built and the machine performance predictions generated for various loading conditions including no-load operation. The specifications and off-line testing results for the experimental verification of the theoretical analyses of the manufactured BEESRGs with the 4-pole and 6-pole rotor prototypes of the aforementioned types are presented in Section V. Finally, Section VI has summarized the main conclusions and/or insightful remarks from the research being undertaken.

II. Theoretical Analysis of BEESRG

A. Operation principle

The BEESRG is a novel and upgraded version of the EESG, but its structure and torque producing mechanism are entirely different from the traditional concept. As shown in Fig. 1, the BEESRG has two sets of stator windings and a brushless rotor unlike the conventional wound rotor EESG. The 2p-pole AW is used for power generation, whereas the 2q-pole EW is DC fed from the excitation system. The AW and EW generate the rotating and stationary magnetic fields in the air-gap, respectively, the magnetic coupling and consequent torque production being achieved by their interactions with the flux components coming from the rotor modulating action. In steady-state, the rotor speed (rev/min) can be expressed as:

$$n_r = \frac{60f}{p+q} \tag{1}$$

where the number of rotor poles p_r=p+q is equal to the total pole-pair number of both stator windings in contrast with the EESG. This means that the BEESRG speed is half that of the equivalent p_r-pole EESG or DFIG for the same AW frequency.

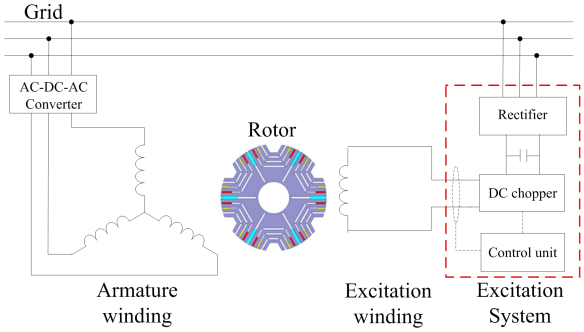

Fig. 1. A simplified structural diagram of the grid-connected BEESRG.

The excitation system in Fig. 1 consists of three parts: Rectifier, IPM (e.g. a DC chopper), and a control unit. A typical converter topology is shown in Fig. 2. A similar full-scale power converter design but with two additional inverter legs for 3-phase grid connection of the AW has been used as per Fig. 1.

In the BEESRG, the rotor construction basically determines the level of magnetic coupling between the stator windings, and in turn, the machine performance. The common rotor can appear in three distinct forms: the cage rotor, the wound rotor, and the modern reluctance rotor [18-23]. The merits and demerits of various rotor designs have been comparatively

analyzed in [24]. Considering the coupling capacity and manufacturing process synthetically, the magnetic barrier and hybrid rotors illustrated in Fig. 3 are researched in this paper.

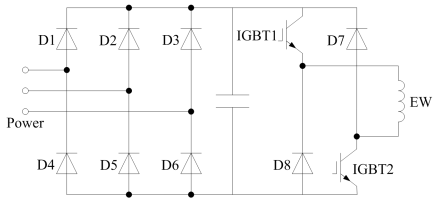

Fig. 2. The excitation converter configuration.

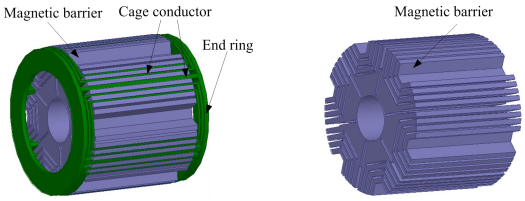

Fig. 3. 3-D models of the hybrid rotor (left) and magnetic barrier rotor (right).

B. Power flow

Assume that the slip power contributions of the AW and EW in steady-state are P_{sAW} and P_{sEW}, respectively. Because the rotor resistance is small, the rotor copper losses can be ignored, and the slip power relationship can be expressed as:

$$P_{sAW} + P_{sEW} = 0 \tag{2}$$

According to (2), P_{sAW} and P_{sEW} are the same, but the direction of power flow in the two windings is opposite.

The electromagnetic power and slip expressions are of standard induction machine form and can be written as:

$$P_{emAW} = \frac{P_{sAW}}{s_{AW}} < 0 \qquad P_{emEW} = \frac{P_{sEW}}{s_{EW}} \to 0 \tag{3}$$

$$s_{AW} = \frac{n_{AW} - n_r}{n_{AW}} \qquad s_{EW} = \frac{n_{EW} - n_r}{n_{EW}} \tag{4}$$

Note that whilst s_{AW} is ranging from of 0 to 1, s_{EW} is tending to infinity as the DC magnetic field of the EW is stationary i.e. $n_{EW} = 0$ in (4).

The mechanical and other power relationships of interest that can be derived using (2) and (3) are as follows [25]:

$$\left.\begin{aligned} P_{mecAW} &= (1 - s_{AW})\, P_{emAW} < 0 \\ P_{mecEW} &= (1 - s_{EW})\, P_{emEW} = (s_{AW} - \frac{s_{AW}}{s_{EW}})\, P_{emAW} < 0 \end{aligned}\right\} \tag{5}$$

$$\left.\begin{aligned} P_{sEW} &= -P_{sAW} = -s_{AW} P_{emAW} > 0 \\ P_{emEW} &= \frac{P_{sEW}}{s_{EW}} = -\frac{P_{sAW}}{s_{EW}} = -\frac{s_{AW}}{s_{EW}} P_{emAW} \to 0 \end{aligned}\right\} \tag{6}$$

Fig. 4 shows a power flow diagram of the BEESRG corresponding to (5) and (6) above.

III. Coupling Capacity of BEESRG

As for any other machine, the degree of magnetic coupling is critical to the BEESRG performance, and as such it represents one of the key optimization parameters in the design process. The implications of various pole combinations, the EW pole number, and the rotor dimensions on magnetic coupling properties of the BEESRG are considered in this section.

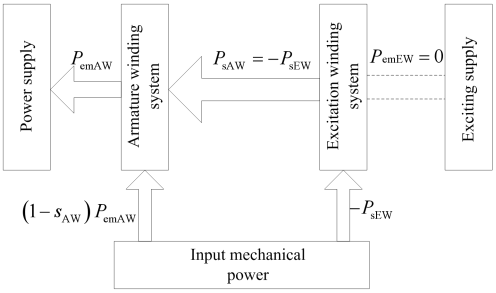

Fig. 4. A power flow chart of the BEESRG.

A. Pole combination

Various pole combinations can lead to different coupling capacities, and hence the achievable performance of the BEESRG [21]. In the selection process, the following principles should be observed and/or the relationships satisfied:

- In order to avoid direct coupling between the AW and EW, p and q must be different.
- In order to reduce the radial pull and vibration, the windings pole-pairs should be such that $|p - q| \geq 2$ [26].
- In order to maximize the power density, $|p - q|$ should be made as small as possible when $p + q$ is constant [27].

In keeping with the above constraints, 6/2 pole, 8/2 pole, and 8/4 pole combinations are analyzed and compared, assuming the lower pole number for the EW. The respective relative harmonic diagrams obtained by the Fourier decomposition of the air-gap flux density are shown in Fig. 5, where the harmonic order of the AW pole-pair number has been identified as useful, and the EW counterpart as the fundamental component used as a base for normalization (e.g. 100%). For example, the useful harmonic for the 6/2 pole case in Fig. 5a is of the 3rd order (i.e. 6/2), whereas the fundamental is of the 1st order (i.e. 2/2).

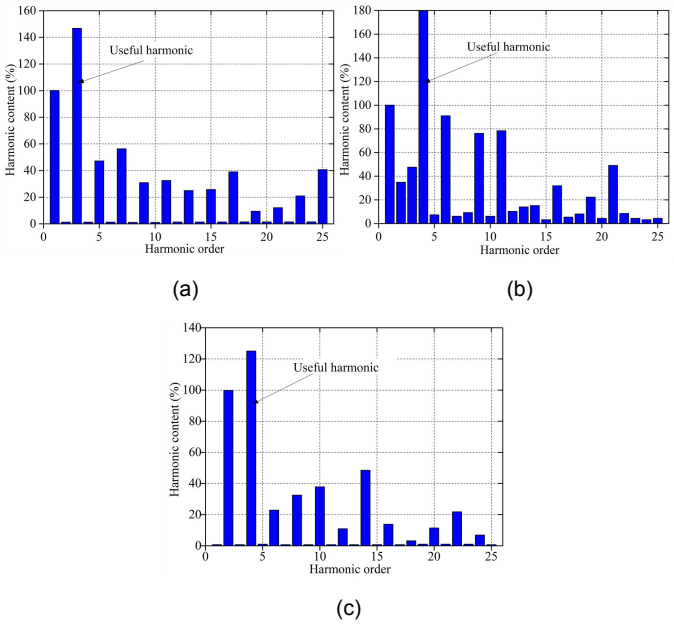

Fig. 5. Spectrum diagram of the air-gap flux density for different BEESRG pole combinations: (a) 6/2 pole; (b) 8/2 pole; (c) 8/4 pole.

From Fig. 5, it can be noticed that for the 8/2 pole windings, the 4th harmonic content is up to 180%, but the parasitic

This article has been accepted for publication in a future issue of this journal, but has not been fully edited. Content may change prior to final publication. Citation information: DOI 10.1109/TIE.2018.2821109, IEEE Transactions on Industrial Electronics

components, such as the 6th, 9th, and 11th, are also rather high, even exceeding 80%. Therefore, the asymmetrical 5-pole rotor structure results in an increase of undesirable harmonics. In contrast, the useful 3rd and 4th harmonic for the 6/2 pole and 8/4 pole BEESRGs, respectively, are proportionally smaller, the useless harmonics, however, being much less in content than in Fig. 5b. Hence, the 6/2 and 8/4 pole winding combinations will be investigated further as more promising.

B. Excitation winding pole pair number

When compared with more traditional machines, the BEESRG structure is relatively complex. The stator windings of different pole numbers have two-fold functions, i.e., excitation and/or torque production. However, there is no adopted consensus as to which winding should be primarily flux or torque producing. In order to examine the BEESRG performance in this sense, two excitation modes of the 6/2 pole and 8/4 pole BEESRG are compared by Fourier analysis. The corresponding spectrum diagrams are shown in Figs. 6 and 7.

When the EW is only supplied, the greater the harmonic component of the same order as the AW pole-pair number, the stronger the coupling capacity of the BEESRG. Note from Figs. 6 and 7 that the useful harmonic content of the excitation mode where the EW has a fewer pole number (e.g. 2-pole in Fig. 6 and 4-pole in Fig. 7) is higher than if the other winding with more poles is used for the same purpose (e.g. 6-pole in Fig. 6 and 8-pole in Fig. 7). So, when the fewer pole winding is largely flux producing, the magnetic coupling is better. This winding is therefore used as the EW in the further studies.

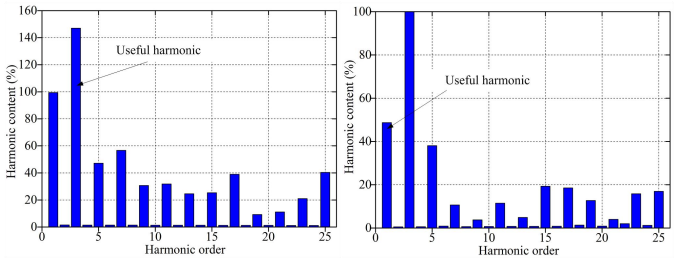

Fig. 6. Harmonic spectrum diagram of air-gap flux density for 2-pole winding excitation (left) and 6-pole winding excitation (right).

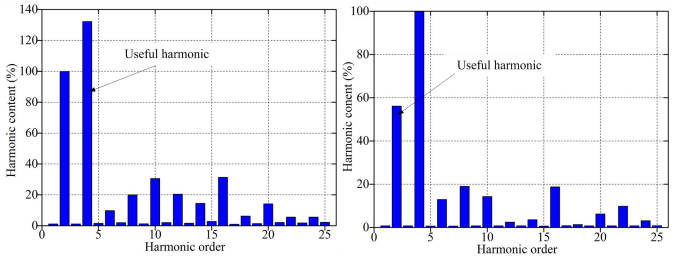

Fig. 7. Spectrum diagrams of air-gap flux density harmonic for 4-pole winding excitation (left) and 8-pole winding excitation (right).

C. Effects of rotor parameters

The magnetic interaction between the AW and EW is realized through the rotor modulating action. The rotor design optimization is thus of utmost importance for the BEESRG performance [28-29]. The main parameters to specifically look at are the pole-arc coefficient, the magnetic layer number, the ratio of magnetic and non-magnetic layers, and the number of cage conductors. The influence of these parameters on the coupling capacity of the 8/4 pole BEESRG with a 6-pole rotor depicted in Fig. 8 will be investigated in the following.

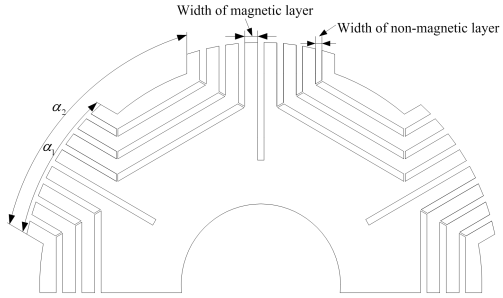

Fig. 8. A structural diagram of the BEESRG reluctance rotor.

1) Pole arc coefficient

The pole arc coefficient (PAC) directly determines the air gap length between two adjacent salient poles, and as such is very important for the magnetic coupling. It can be expressed as α_1/α_2 where the meanings of α_1 and α_2 are defined in Fig. 8. As shown in Fig. 9, with the increasing PAC, the ratio of useful and fundamental harmonic components (i.e. the harmonic content) decrease. Given that a number of magnetic barriers are required to be inserted, selecting a small PAC value can cause the rotor magnetic circuit to saturate easier, and its mechanical sturdiness would also be compromised. Therefore, the PAC is chosen to be 0.7 as a trade-off.

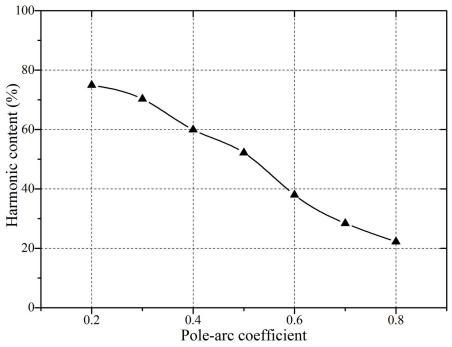

Fig. 9. Effect of pole arc coefficient on the magnetic coupling capacity.

2) Magnetic layer number

A magnetic barrier rotor is composed of both magnetic and non-magnetic layers. By increasing their number, the magnetic anisotropy would increase, thus enhancing the level of magnetic field modulation, but at the expense of manufacturing difficulties (and hence higher cost) and mechanical robustness of the entire rotor construction (i.e. it would become more flimsy with a high number of punched laminations). As illustrated in Fig. 10, with the rise of the magnetic layer number, the relative useful harmonic content also increases as expected. However, when the magnetic layer number is over 4, the coupling capacity has nearly reached the saturation showing no apparent signs of further improvement.

This article has been accepted for publication in a future issue of this journal, but has not been fully edited. Content may change prior to final publication. Citation information: DOI 10.1109/TIE.2018.2821109, IEEE Transactions on Industrial Electronics

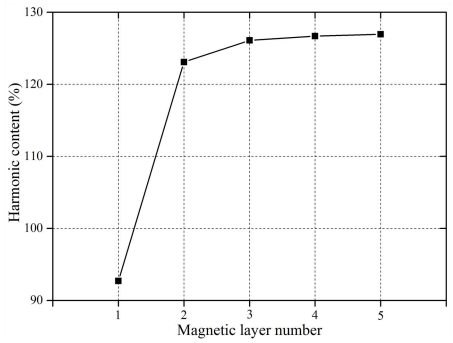

Fig. 10. Effect of magnetic layer number on coupling capacity.

3) Ratio of magnetic and non-magnetic layer

The non-magnetic layer can guide the magnetic flux of the machine. Therefore, it is important to carefully select the ratio of magnetic and non-magnetic layer widths (λ) annotated in Fig. 8. Four simulation models with the ratios of 1, 1.5, 2, and 2.5, are established and individually simulated to obtain the relative useful harmonic content (β) normalized to the fundamental component. As tabulated in Table I, β exhibits the rising trend with the increasing λ up to the value of 5:2 when it begins to decrease. Therefore, for $\lambda = 2$ (i.e. 2:1), the coupling capacity is the strongest.

TABLE I
EFFECT OF MAGNETIC AND NON-MAGNETIC LAYERS RATIO ON MAGNETIC COUPLING CAPACITY

Ratio of magnetic and non-magnetic layer	β (%)
1:1	116.93
3:2	120.68
2:1	124.95
5:2	119.86

4) Cage conductor number

Cage conductors i.e. a common cage conductor (CCC) and a short-circuit cage conductor (SCCC), can improve the coupling capacity of a magnetic barrier rotor. Both CCC and SCCC are similar to ordinary squirrel-cage rotor bars as shown in Fig. 11. In this section, four case studies (i.e. one CCC on its own and then together with, one, two or three SCCCs) have been analyzed. The respective 3-D structures are shown in Fig. 12 with the corresponding variations of 4-pole and 8-pole magnetic field components appearing in Fig. 13.

According to Fig. 13, it can be seen that with the number of CCC increasing, the values of 8-pole magnetic field component increase gradually, while the 4-pole counterparts decrease. When the SCCC number is from 2 (Case 3) to 3 (Case 4), the coupling capacity of the BEESRG has no obvious enhancement. However, the downside of increasing the SCCC number is that the manufacturing cost and rotor copper losses would likewise go up. As a good compromise, the Case 3 (i.e. a single CCC and two SCCCs) is selected eventually.

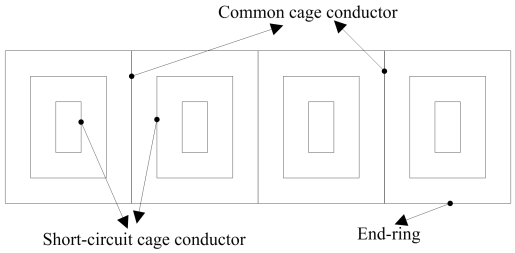

Fig. 11. An outline of the nested-loop cage rotor.

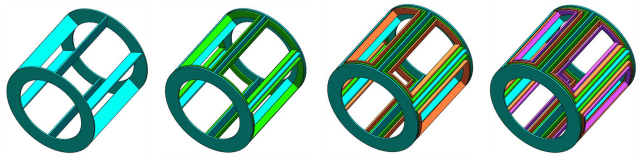

(Case 1) (Case 2) (Case 3) (Case 4)

Fig. 12. Different 3D-structures of cage rotors with: (Case 1) A common cage conductor (CCC) only; (Case 2) A CCC and one short-circuit cage conductor (SCCC); (Case 3) A CCC and two SCCCs;. (Case 4) A CCC and three SCCCs.

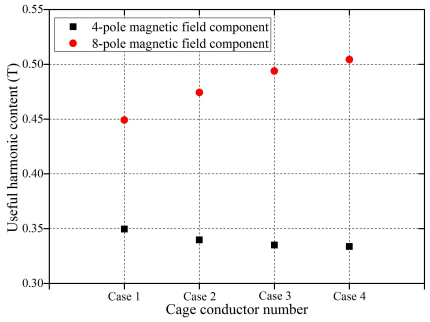

Fig. 13. Effects of cage conductor number on the coupling capacity.

IV. BEESRG PERFORMANCE ANALYSIS

The 2-D simulation models for the four BEESRG prototypes (i.e., two stators and four rotors) are built. The specifications of the prototypes used to produce the results presented in this section are given in Table II.

TABLE II
THE MAIN PARAMETERS OF THE BEESRG PROTOTYPES

Parameters (Unit)	6-pole rotor	4-pole rotor
Rated power (kW)	11	15
Rated voltage (V)	380	380
Pole pair number	[8, 4]	[6, 2]
Rated frequency (Hz)	50	50
Rated speed (r/min)	500	750
Stator outer diameter (mm)	400	400
Stator inner diameter (mm)	285	260
Slot number	72	54
Air gap width (mm)	0.5	0.8
Core length (mm)	225	240
Rotor inner diameter (mm)	85	85
AW connection	Y	Y
Rotor rib width (mm)	2.5	2.5
Pole arc coefficient	0.7	0.7
Magnetic layer number	4	4
Ratio of magnetic and non-magnetic layer	2:1	2:1
Cage conductor number	3	3

A. No-load characteristics

The speed of the unloaded BEESRG is kept at synchronous value with the DC fed excitation winding (EW). The respective no-load curves are shown in Fig. 14. It can be seen that the AW open-circuit (induced) voltage increases with the raise of the EW currents (and hence related flux magnitudes) as expected. Note that for the same excitation current, the voltage levels of the BEESGs with the hybrid rotor are notably higher than using the magnetic barrier rotor. Therefore, the mutual inductance values and magnetic coupling capacity provided by the hybrid rotor are clearly superior.

This article has been accepted for publication in a future issue of this journal, but has not been fully edited. Content may change prior to final publication. Citation information: DOI 10.1109/TIE.2018.2821109, IEEE Transactions on Industrial Electronics

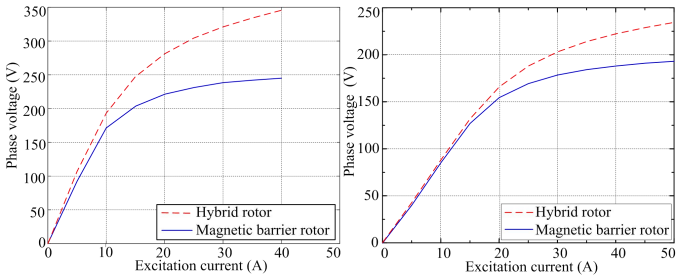

Fig. 14. Simulated no-load characteristics of the 8/4 pole (left) and 6/2 pole (right) BEESRGs.

The air gap flux density waveforms of the 6/2 pole and 8/4 pole BEESRGs with the magnetic barrier and hybrid rotors are shown in Fig. 15 and 16, respectively.

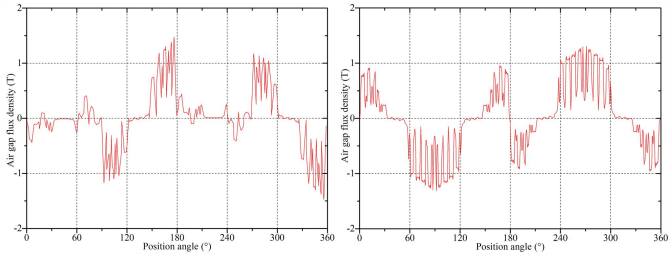

Fig. 15. Waveforms of air gap flux density of the 6/2 pole BEESRGs with the magnetic barrier rotor (left) and hybrid rotor (right).

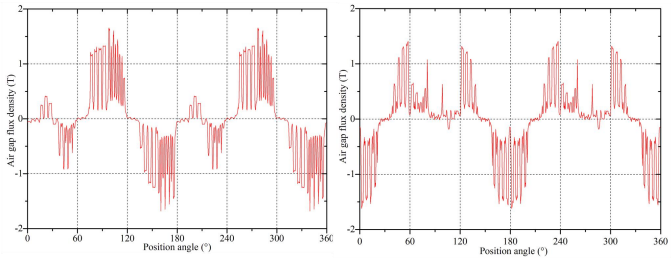

Fig. 16. Waveforms of air gap flux density of the 8/4 pole BEESRGs with the magnetic barrier rotor (left) and hybrid rotor (right).

B. Short-circuit characteristics

The short-circuit characteristics of the BEESRGs with the AW shorted are shown in Figs. 17 and 18. It can be seen that the armature current increases with the rising excitation current in a nearly linear fashion indicating largely unsaturated magnetic circuit conditions.

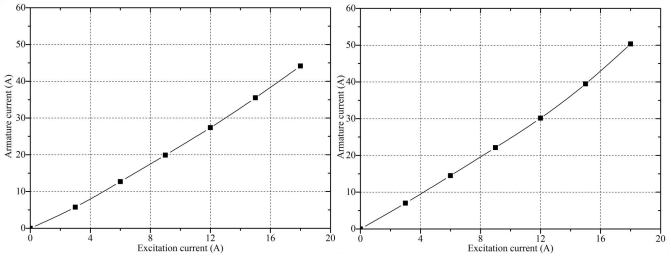

Fig. 17. Short circuit characteristic of the 6/2 pole BEESRGs with the magnetic barrier rotor (left) and the hybrid rotor (right).

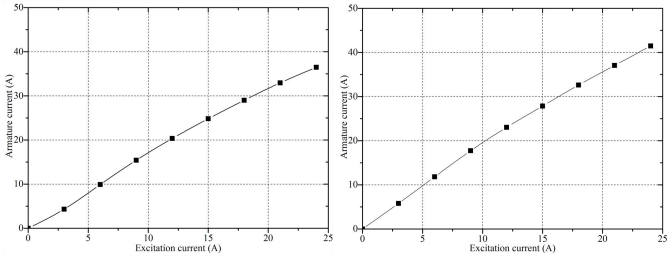

Fig. 18. Short circuit characteristic of the 8/4 pole BEESRGs with the magnetic barrier rotor (left) and the hybrid rotor (right).

C. Loading characteristics

Given that the coupling capacities of the two rotors differ, so will the rated voltages even when the stator diameter and the windings are completely identical. When the AW is connected to a purely resistive load, the terminal voltage should be maintained constant by appropriately adjusting the EW current.

1) 6/2 pole design

The voltage and current curves for the BEESRGs with two different rotors at 5 kW output power are presented in Figs. 19 and 20. It can be observed that both waveforms are essentially sinusoidal in nature, but with a notable DC voltage offset. The underlying reason should be that the AW pole number is an odd multiple (6/2 = 3) of the EW pole number, which induces lots of harmonics for this particular design type.

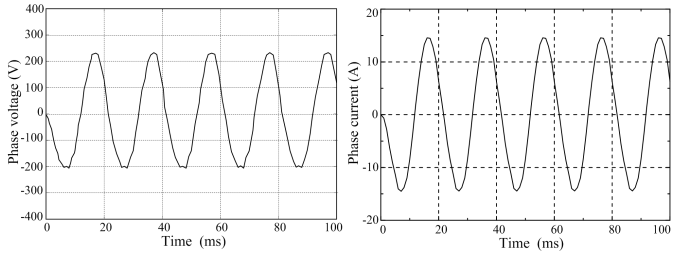

Fig. 19. Voltage and current waveforms of the loaded 6/2 pole BEESRG with the magnetic barrier rotor.

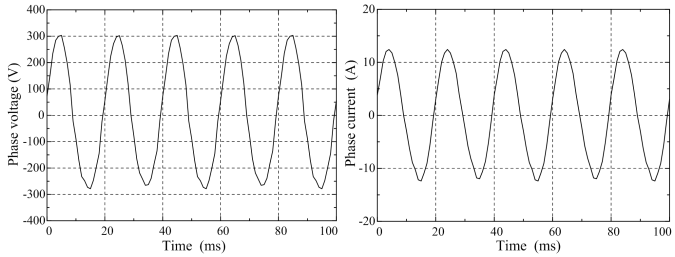

Fig. 20. Voltage and current waveforms of the loaded 6/2 pole BEESRG with the hybrid rotor.

Figs. 21 and 22 show the corresponding flux line and magnetic density distributions, whereas Fig. 23 illustrates the air-gap flux density harmonic content. It can be seen that the 4-pole distribution of the hybrid rotor is much more pronounced than that of the magnetic barrier rotor as a result of the stronger magnetic field modulation capacity.

This article has been accepted for publication in a future issue of this journal, but has not been fully edited. Content may change prior to final publication. Citation information: DOI 10.1109/TIE.2018.2821109, IEEE Transactions on Industrial Electronics

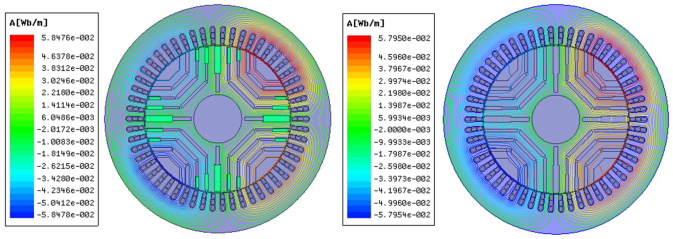

Fig. 21. Flux line distribution of the loaded 6/2 pole BEESRG with the hybrid rotor (left) and magnetic barrier rotor (right).

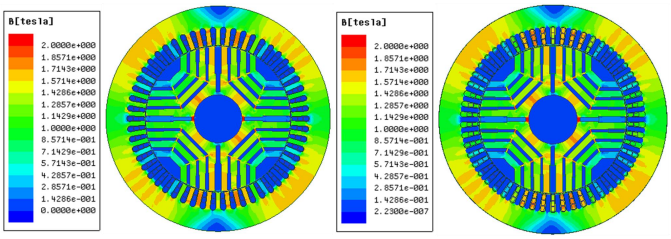

Fig. 22. Magnetic density distribution of the loaded 6/2 pole BEESRG with the magnetic barrier rotor (left) and hybrid rotor (right).

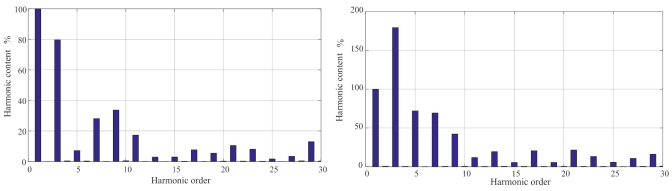

Fig. 23. Harmonic spectrum diagram of the air-gap flux density for the 6/2 pole BEESRG with the magnetic barrier (left) and hybrid rotor (right).

In order to analyze the VRR, the voltage-current relationship of the AW is investigated. As shown in Fig. 24, the VRR of the 6/2 pole BEESRG with the hybrid rotor (red line) is 9.1%.

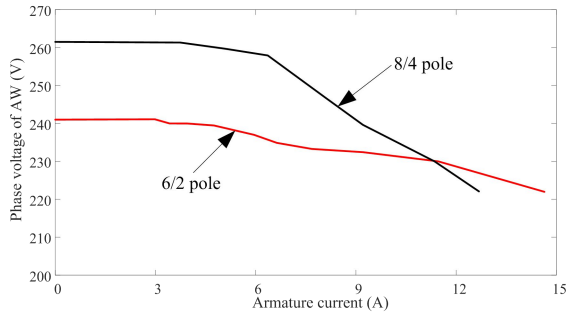

Fig. 24. External characteristic of the 6/2 pole and 8/4 pole BEESRG with the hybrid rotor.

2) 8/4 pole design

The voltage and current waveforms for the 8/4 pole BEESRGs at 5 kW are shown in Figs. 25 and 26. Again, these are largely sinusoidal in shape, but unlike the 6/2 pole equivalents in Figs. 19 and 20, there is no superimposed DC voltage component. This can be explained by the fact that the AW pole number is now an even multiple (8/4 = 2) of that of the EW, and there is little harmonics generated, which makes this pole arrangement a preferable choice from this point of view.

Figs. 27 and 28 show the respective flux line and magnetic density distributions, and Fig. 29 plots the air-gap flux density harmonic content, of the loaded 8/4 pole BEESRGs. The same conclusion of the hybrid rotor being able to offer the stronger magnetic field modulation than the magnetic barrier rotor can also be made as in the 6/2 pole case.

For VRR comparisons of the BEESRGs with two different pole combinations, the relation between the phase voltage and current of the 8/4 pole BEESRG with the hybrid rotor is plotted in the same Fig. 24 (black line). Notice that the VRR of 17.9 % is nearly double the value of the 6/2 pole counterpart.

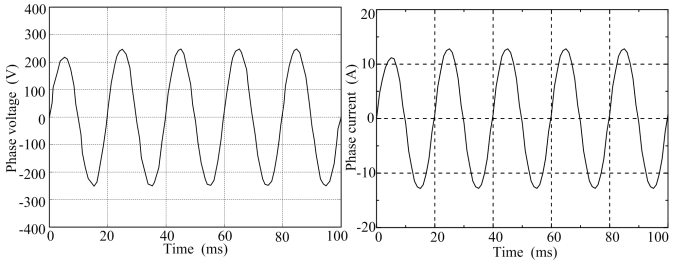

Fig. 25. Voltage and current waveforms of the loaded 8/4 pole BEESRG with the magnetic barrier rotor.

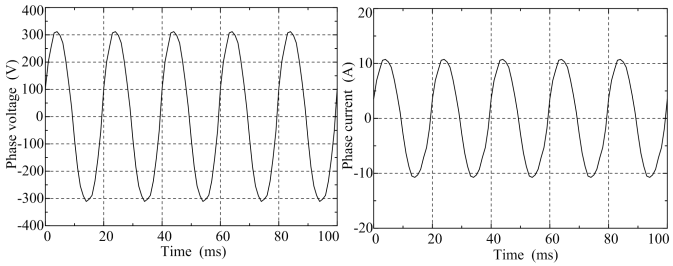

Fig. 26. Voltage and current waveforms of the loaded 8/4 pole BEESRG with the hybrid rotor.

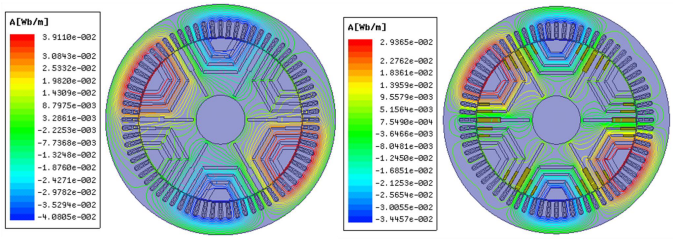

Fig. 27. Flux line distribution of the loaded 8/4 pole BEESRG with the magnetic barrier rotor (left) and the hybrid rotor (right).

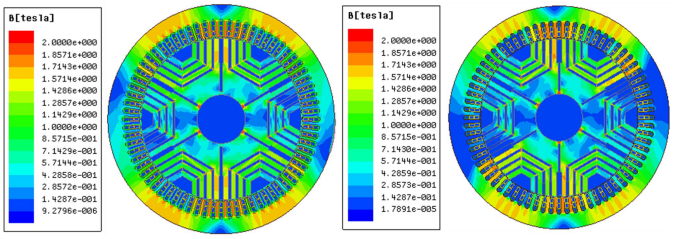

Fig. 28. Magnetic density distribution of the loaded 8/4 pole BEESRG with the magnetic barrier rotor (left) and the hybrid rotor (right).

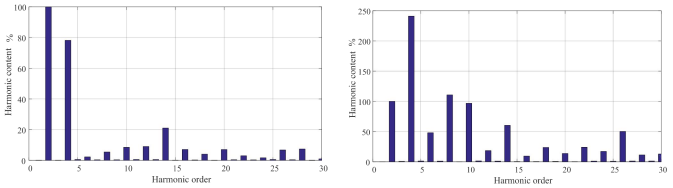

Fig. 29. Harmonic spectrum diagram of the air-gap flux density for the 8/4 pole BEESRG with the magnetic barrier (left) and hybrid rotor (right).

This article has been accepted for publication in a future issue of this journal, but has not been fully edited. Content may change prior to final publication. Citation information: DOI 10.1109/TIE.2018.2821109, IEEE Transactions on Industrial Electronics

V. Experimental Studies

The prototype 6/2 pole and 8/4 pole BEESRGs with the hybrid and magnetic barrier rotors (Fig. 30) have been built and tested for the verification of the simulation results. A photo of the experimental test system is shown in Fig. 31.

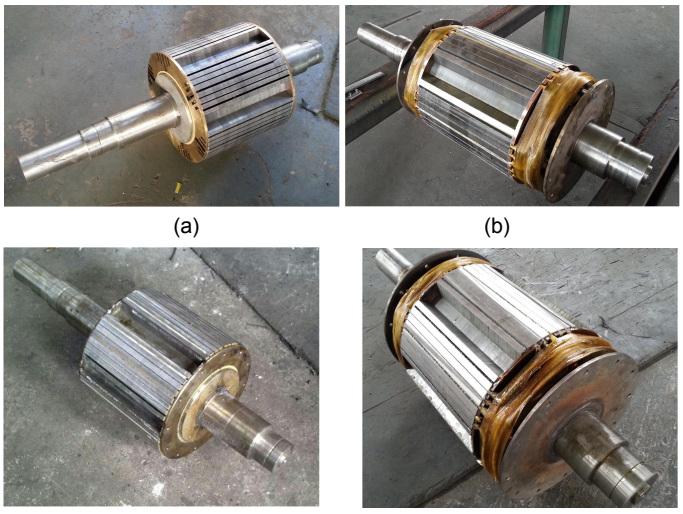

Fig. 30. Four rotor prototypes for the 6/2 pole and 8/4 pole BEESRGs: (a) 4-pole magnetic barrier rotor; (b) 4-pole hybrid rotor; (c) 6-pole magnetic barrier rotor; (d) 6-pole hybrid rotor.

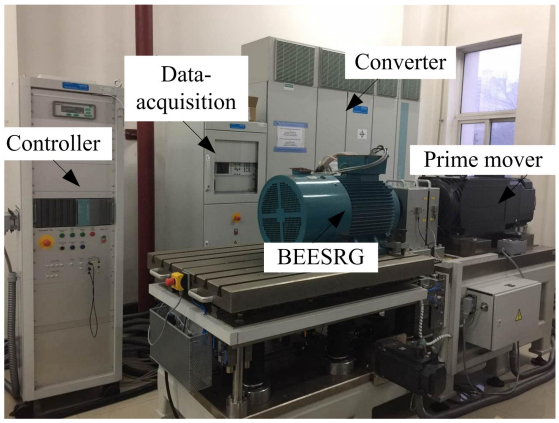

Fig. 31. The BEESRG test rig used for the experimental studies.

A. Measurement of mutual inductance

The BEESRG torque expression is basically the same as for the BDFG and can be written as follows [30]:

$$T_{\text{em}} = \frac{3}{2}\cdot(p+q)\cdot L\cdot i_{AW}\cdot i_{EW}\cdot\sin\gamma \qquad (7)$$

It is clear from (7) that L plays an important role in the torque production of the machine. This is measured at standstill with one phase of the AW being AC excited, and the other winding open circuited. The measurements obtained for the 6/2 pole and 8/4 pole BEESRGs with 4-pole and 6-pole rotors respectively are shown in Fig. 32.

It can be seen from Fig. 32 that the peak-to-peak value of the BEESRG mutual inductance with the hybrid rotor is about 50% higher than with the magnetic barrier rotor owing to the stronger coupling capacity. Furthermore, note that the mutual inductance waveforms of the 8/4 pole BEESRGs do not have a DC component, unlike the 6/2 pole designs by analogy to the simulated voltage counterparts in Figs. 12-13 and 15-16.

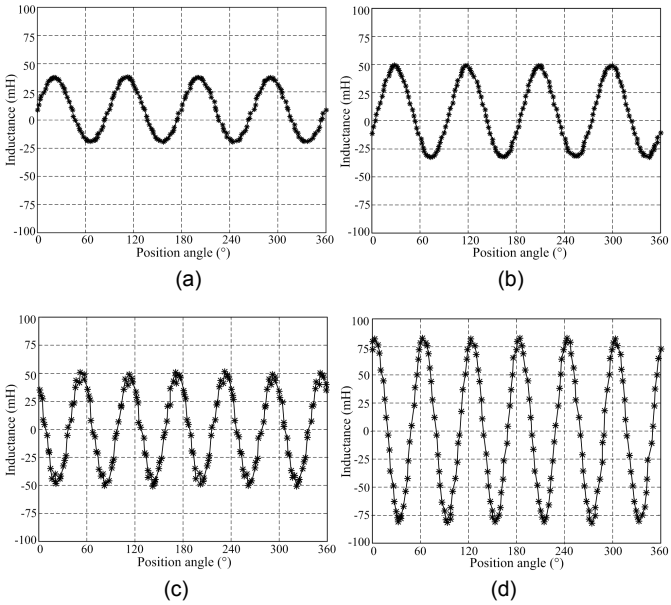

Fig. 32. Measured mutual inductance of the BEESRG with: (a) 4-pole magnetic barrier rotor; (b) 4-pole hybrid rotor; (c) 6-pole magnetic barrier rotor; (d) 6-pole hybrid rotor.

B. No-load tests

The no-load curves of the 6/2 pole and 8/4 pole BEESRGs with different rotors are presented in Fig. 33. As shown, whether 6/2 pole or 8/4 pole BEESRG, the AW terminal voltage with the hybrid rotor is higher than with the magnetic barrier rotor under the same operating conditions suggesting the stronger coupling capacity of hybrid rotor similarly to the simulation results in Fig. 14.

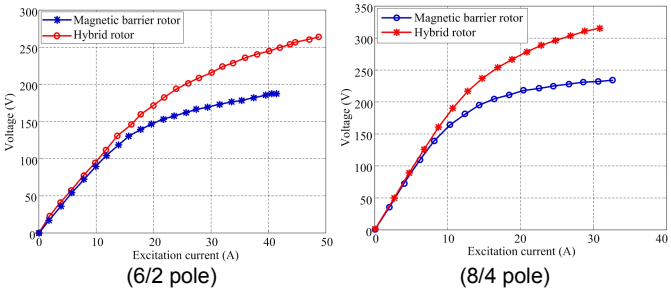

Fig. 33. Measured no-load characteristics of the BEESRG prototypes.

C. Load tests

The BEESRGs are tested under different loading conditions so that the efficiency can be measured. As shown in Fig. 34, the efficiency of the 6/2 pole BEESRG with the magnetic barrier and hybrid rotors is 81.3% and 80.4% at 14.6kW, the maximum output powers being 14.6 kW and 16.7 kW, respectively. Similarly, the corresponding efficiencies of the 8/4 pole BEESRG are 81.2% and 80.4% at 10kW, with the maximum output powers being 10.7 kW and 14.3 kW, respectively. In conclusion, whether 6/2 pole or 8/4 pole designs, the BEESRG efficiency with magnetic barrier rotor is slightly better than using the hybrid rotor for the same power delivered. However, the maximum output power of the BEESRGs with the hybrid rotor is clearly higher than with the magnetic barrier rotor. The

experimental results verify that the hybrid rotor can offer much stronger overload capacity.

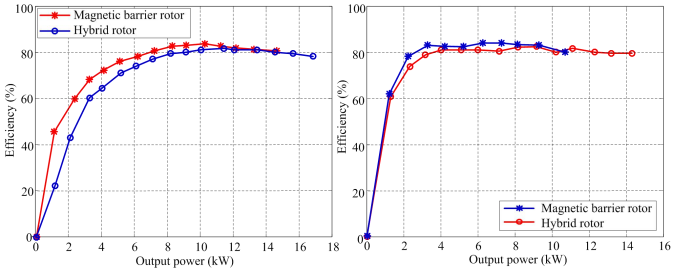

Fig. 34. Efficiency curves of the BEESRG prototypes.

The voltage and current measurements for the four prototype machines producing 5 kW are presented in Fig. 35 and 36. As shown in Fig. 35, the waveforms of the 6/2 pole BEESRG have a dc component, and are distorted to some extent. Conversely, it can be seen from Fig. 36 that the respective waveforms of the 8/4 pole BEESRG are much cleaner and with no DC offset.

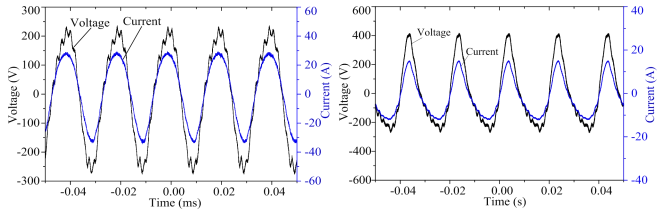

Fig. 35. Current and voltage waveforms of the 6/2 pole BEESRG prototypes with the magnetic barrier rotor (left) and hybrid rotor (right).

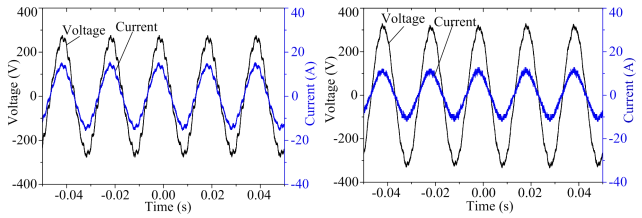

Fig. 36. Current and voltage waveforms of the 8/4 pole BEESRG prototypes with the magnetic barrier rotor (left) and hybrid rotor (right).

VI. Conclusions

This paper has presented the detailed design studies and thorough analysis of the novel BEESRG with the magnetic barrier reluctance rotors and cage assisted hybrid rotors. Four machine prototypes with 6/2 pole and 8/4 pole wounded stators and 4 pole or 6 pole rotors of each type have been custom built, simulated, and laboratory tested. The following important conclusions and/or observations can be made from the comprehensive simulation and experimental results produced:

- The lower pole (excitation) winding is more suited for the magnetization purposes, and the higher pole (armature) winding for torque (power) production. Such an arrangement offers the desirable harmonic content and better magnetic coupling to the machine for either pole combination considered (i.e. 6/2 or 8/4).
- The magnetic coupling and overload capacities of the BEESRG with the hybrid rotor are much stronger than with the magnetic barrier rotor, although the latter offers a somewhat better efficiency for the same output power.
- The percentage voltage regulation rate of the 6/2 pole BEESRGs is almost half that of the 8/4 pole one.
- The quality of the current and voltage waveforms of the 8/4 pole BEESRG is clearly superior to the 6/2 pole counterpart, with the hybrid rotor in particular. Therefore, the 8/4 pole windings option is generally more preferable for the BEESRG.

References

[1] M. Cheng, W. Hua, J. Zhang, and W. Zhao, "Overview of stator-permanent magnet brushless machines," *IEEE Trans. Ind. Electron.*, vol. 58, DOI: 10.1109/TIE.2011.2123853, no. 11, pp. 5087-5101, Nov. 2011.

[2] F. Yao, Q. An, L. Sun, and T. A. Lipo, "Performance investigation of a brushless synchronous machine with additional harmonic field windings," *IEEE Trans. Ind. Electron.*, vol. 63, DOI: 10.1109/TIE.2016.2581759, no. 11, pp. 6756-6766, Nov. 2016.

[3] P. Bajec, B. Pevec, D. Voncina, D. Miljavec, and J. Nastran, "Extending the low speed operation range of PM generator in automotive applications using novel AC-DC converter control," *IEEE Trans. Ind. Electron.*, vol. 52, DOI: 10.1109/TIE.2005.843912, no. 2, pp. 436-443, Apr. 2005.

[4] C. T. Mi, M. Filippa, J. Shen, and N. Natarajan, "Modelling and control of a variable-speed constant-frequency synchronous generator with brushless exciter," *IEEE Trans. Ind. Appl.*, vol. 40, DOI: 10.1109/TIA.2004.824504, no. 2, pp. 565-573, Mar./Apr. 2004.

[5] K. Hu, X. M. Deng, and F. Y. He, "Design and analysis of novel structure brushless electrically excited synchronous motor," *Electr. Mach. Control*, vol. 18, DOI：10.15938/j.emc.2014.01.014, no. 1, pp. 86-91, Jan. 2014.

[6] J. Wei, Q. Zheng, and Y. Yang, "Integrated AC and DC excitation method for brushless synchronous machine," *Proc. IEEE ECCE*, Raleigh, NC, USA, DOI: 10.1109/ECCE.2012.6342465, pp. 2322-2325, Mar. 2012.

[7] Z. Q. Zhu, and X. Liu, "Novel stator electrically field excited synchronous machines without rare-earth magnet," *IEEE Trans. Magn.*, vol. 51, DOI: 10.1109/TMAG.2014.2355177, no. 1, pp. 1-9, Apr. 2015.

[8] P. Han, M. Cheng, Y. L. Jiang, and Z. Chen, "Torque/power density optimization of a dual stator brushless doubly fed induction generator for wind power application," *IEEE Trans. Ind. Electron.*, vol. 64, DOI: 10.1109/TIE.2017.2726964, no. 12 , pp. 9864-9875, Dec. 2017.

[9] F. Yao, Q. T. An, L. Z. Sun, and T. A. Lipo, "Performance investigation of a brushless synchronous machine with additional harmonic field windings," *IEEE Trans. Ind. Electron.*, vol. 63, DOI: 10.1109/TIE.2016.2581759, no. 11, pp. 6756-6766, Nov. 2016.

[10] J. G. Bai, P. zheng, C. D. Tong, Z. Y. Song, and Q. B. Zhao, "Characteristic analysis and verificationof the magnetic-field-modulated brushless double-rotor machine," *IEEE Trans. Ind. Electron.*, vol. 62, DOI: 10.1109/TIE.2014.2381159, no. 7 , pp. 4023-4033, Dec. 2014./ Jul. 2015.

[11] A. C. Pop, J. J. C. Gyselinck, D. E. Pinto, I. Vintiloiu, "Optimization of low-power brushless PM-machines for automotive applications with focus on high-volume mass production," *IEEE Trans. Ind. Electron.*, vol. 64, DOI: 10.1109/TIE.2017.2698367, no. 12 , pp. 9767-9775, Jun. 2017.

[12] E. Bostanci, Z. Neuschl, R. Plikat, and B. Ponick, "No-load performance analysis of brushless DC machines with axially displaceable rotor," *IEEE Trans. Ind. Electron.*, vol. 61, DOI: 10.1109/TIE.2013.2263781, no. 4, pp. 1692-1699, Apr. 2014.

[13] C. D. Tong, P. Zheng, Q. Wu, J. G. Bai, and Q. B. Zhao, "A brushless claw-pole double-rotor machine for power-split hybrid electric vehicles," *IEEE Trans. Ind. Electron.*, vol. 61, DOI: 10.1109/TIE.2013.2281169, no. 8 , pp. 4295-4305, Aug. 2014.

[14] J. J. Dai, S. Hagen, D. C. Ludois, and I. P. Brown, "Synchronous generator brushless field excitation and voltage regulation via capacitive coupling through journal bearings," *IEEE Trans. Ind. Appl.*, vol. 53, DOI: 10.1109/TIA.2017.2681621, no. 4, pp. 3317-3326, Jul. 2017.

[15] C. Stancu, T. Ward, K. Rahman, R. Dawsey, and P. Savagian, "Separately excited synchronous motor with rotary transformer for hybrid vehicle application," *IEEE Trans. Ind. Appl.*, DOI: 10.1109/TIA.2017.2757019, Sep. 2017.

[16] A. D. Gioia, I. P. Brown, Y. Nie, R. Knippel, D. C. Ludois, J. J. Dai, S. Hagen, and C. Alteheld, "Design of a wound field synchronous machine for electric vehicle traction with brushless capacitive field excitation," *Proc. IEEE ECCE*, Milwaukee, WI, USA, DOI: 10.1109/ECCE.2016.7855023, pp. 1-8, Sep. 2016.

[17] R. A. McMahon, M. E. Mathekga, X. Y. Wang, and M. R. Tatlow, "Design considerations for the brushless doubly fed (induction) machine," *IET Electr. Power Appl.*, vol. 10, DOI: 10.1049/iet-epa.2015.0405, no. 5, pp.394-402, May 2016.

[18] F. Xiong, and X. F. Wang, "Design of a low-harmonic-content wound rotor for the brushless doubly fed generator," *IEEE Trans. Energy Convers.*, vol. 29, DOI: 10.1109/TEC.2013.2287908, no. 1, pp. 158-168, Mar. 2014.

[19] A. Oraee, E. Abdi, S. Abdi, R. McMahon, and P. J. Tavner, "Effects of rotor winding structure on the BDFM equivalent circuit parameters," *IEEE Trans. Energy Convers.*, vol. 30, DOI: 10.1109/TEC.2015.2432272, no. 4, pp.1660-1669, Dec. 2015.

[20] E. Abdi, R. McMahon, P. Malliband, S. Y. Shao, M. E. Mathekga, P. Tavner, S. Abdi, A. Oraee, T. Long, and M. Tatlow, "Performance analysis and testing of a 250 kW medium-speed brushless doubly-fed induction generator," *IET Renew. Power Gener.*, vol.7, DOI: 10.1049/iet-rpg.2012.0234, no.6, pp. 631-638, Nov. 2013.

[21] A. M. Knight, R. E. Betz, and D. G. Dorrell, "Design and analysis of brushless doubly fed reluctance machines," *IEEE Trans. Ind. Appl.*, vol. 49, DOI:10.1109/TIA.2012.2229451, no. 1, pp. 50-58, Jan./Feb. 2013.

[22] M. F. Hsieh, I. H. Lin, and D. Dorrell, "Magnetic circuit modeling of brushless doubly-fed machines with induction and reluctance rotors," *IEEE Trans. Magn.*, vol. 49, DOI: 10.1109/TMAG.2013.2242459, no. 5, pp. 2359-2362, May 2013.

[23] X. Chen, Z. C. Wei, X. M. Gao, C. Y. Ye, and X. F. Wang, "Research of voltage amplitude fluctuation and compensation for wound rotor brushless doubly-fed machine," *IEEE Trans. Energy Convers.*, vol. 30, DOI: 10.1109/TEC.2015.2416515, no. 3, pp. 908-917, Sep. 2015.

[24] F. G. Zhang, S. Y. Yu, H. Wang, Y. T. Wang, and D. P. Wang, "Overview of research and development status of brushless doubly fed machine system," *Chinese J. Electr. Eng.*, vol. 2, DOI: 10.23919/CJEE.2016.7933122, no. 2, pp. 1-13, Dec. 2016.

[25] F. G. Zhang, G. L. Jia, Y. Zheng, and T.Guan, "Characteristic simulation and experimental research of brushless electrically excited synchronous machine," *Trans. China. Electro. Technol. Soc.* vol. 30, no. 14, pp. 100-107, Jul. 2015.

[26] S. Tohidi, M. R. Zolghadri, H. Oraee, P. Tavner, E. Abdi, and T. Logan, "Performance of the brushless doubly fed machine under normal and fault conditions," *IET Electr. Power Appl.*, vol. 6, DOI: 10.1049/iet-epa.2012.0101, no. 9, pp. 621-627, Nov. 2012.

[27] S. C. Yang, "Feature of electromagnetic design for brushless doubly fed machine," *Proceedings of the CSEE*, vol. 21, no. 7, pp. 107-110, 2001.

[28] M. F. Hsieh, Y. H. Chang, and D. G. Dorrell, "Design and Analysis of Brushless Doubly Fed Reluctance Machine for Renewable Energy Applications," *IEEE Trans. Magn.*, vol. 52, DOI: 10.1109/TMAG.2016.2537140, no. 7, pp. 1-5, Mar. 2016.

[29] A. Salman, A. Ehsan, A. Oraee, and R. McMahon, "Equivalent circuit parameters for large brushless doubly fed machines (BDFMs)," *IEEE Trans. Energy Convers.*, vol. 29, DOI: 10.1109/TEC.2014.2311736, no. 3, pp. 706-715, Sep. 2014.

[30] F. X. Wang, F. G. Zhang, and L. Y. Xu, "Parameter and performance comparison of doubly fed brushless machine with cage and reluctance rotors," *IEEE Trans. Ind. Appl.*, vol. 38, vol. 38, DOI: 10.1109/TIA.2002.802917, no. 5, pp. 1237-1243, Sep./Oct. 2002.

Fengge Zhang (M'17) received the B.E.E., M.S., and Ph.D. degrees from the Shenyang University of Technology, Shenyang, China, in 1984, 1990, and 2000, respectively, all in electrical engineering..

Since 1984, he has been with the School of Electrical Engineering, Shenyang University of Technology, where he is currently a Professor. From October 2001 to July 2002, he was a visiting scholar at Esslingen University of Applied Sciences, Esslingen, Germany. He has published numerous journal and conference papers on electrical machines and control systems. His research and teaching interests include electro-magnetic theory, dynamic simulation, magnetic field analysis, optimized design, computer control technology of electrical machines, and wind power generating systems.

Professor Zhang received six paper awards from Liaoning Province and four research awards from the National Machine Industry Ministry, Liaoning Province and Shenyang City, for his outstanding research accomplishments.

Hao Wang received his B.S. and M. S. degrees in Electrical Engineering from Shenyang University of Technology, Shenyang, China, in 2014 and 2017, respectively.

He is currently working toward the Ph.D. degree in Electrical Engineering at Shenyang University of Technology, Shenyang, China. His current research interests include special machine design and wind power generation.

Guanglong Jia received his B.S. and Ph. D. degrees in Electrical Engineering from Shenyang University of Technology, Shenyang, China, in 2010 and 2016, respectively.

He is currently an Engineer with CRRC Zhuzhou Institute Co.Ltd, Zhuzhou, China. His current research interests includes densign of driving motor for new energy vehicles and rail transit.

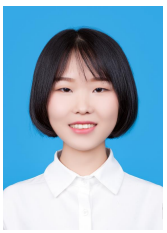

Dandan Ma received her B.S. degree from the Shenyang University of Technology, Shenyang, China, in 2016. She is currently working toward the M.S. degree at Shenyang University of Technology, Shenyang, China.

Her main research interests and activities are in the areas of optimal design, dynamic modelling, simulations and special machine electromagnetic design as well as wind power generation.

Milutin G. Jovanovic (M'99–SM'05) received the Dipl. Eng and M.E.E. degrees from the University of Belgrade, Serbia, in 1987 and 1991, respectively, and the Ph.D. degree from the University of Newcastle, Australia, in 1997, all in electrical power engineering.

He is currently an Associate Professor with the Faculty of Engineering and Environment at Northumbria University Newcastle, Newcastle upon Tyne, United Kingdom. He has published more than 150 journal and conference papers including many book chapters and filed patents. His major interests and activities are in the areas of synchronous reluctance machine drives, power electronics control and applications of doubly-fed motors and/or generators, and wind energy conversion systems.